# X-ray photoelectron spectroscopy of superconducting $RuSr_2Eu_{1.5}Ce_{0.5}Cu_2O_{10}$ and nonsuperconducting $RuSr_2EuCeCu_2O_{10}$

U. Manju,[1] V. P. S. Awana,[2] H. Kishan,[2] and D. D. Sarma[1,3,*]

[1]*Solid State and Structural Chemistry Unit, Indian Institute of Science, Bangalore-560012, India*

[2]*Superconductivity and Cryogenics Division, National Physical Laboratory, Dr. K. S. Krishnan Marg, New Delhi-110012, India*

[3]*Center for Advanced Materials, Indian Association for the Cultivation of Science, Kolkata 700032, India*

(Received 31 July 2006; revised manuscript received 9 October 2006; published 8 December 2006)

We report x-ray photoelectron spectroscopic investigation of $RuSr_2Eu_{1.5}Ce_{0.5}Cu_2O_{10}$ with ferromagnetic $T_C \sim 100$ K and a superconducting transition temperature of $\sim 30$ K compared with $RuSr_2EuCeCu_2O_{10}$, which is a ferromagnetic ($T_C \sim 150$ K) insulator. Our results show that the rare earths, Eu and Ce, are in 3+ and 4+ states, respectively. Comparing the Ru core level spectra from these compounds to those from two Ru reference oxides, we also show that Ru in these ruthenocuprates is always in 5+ state, suggesting that the doped holes in the superconducting compound arising from the substitution of $Ce^{4+}$ by $Eu^{3+}$ are primarily in the Cu-O plane, in close analogy to all other doped high-$T_C$ cuprates. Analysis of Cu $2p$ spectra in terms of a configuration interaction model provides a quantitative description of the gross electronic structures of these ruthenocuprates.

DOI: 10.1103/PhysRevB.74.245106 PACS number(s): 79.60.−i, 74.70.Pq, 71.28.+d, 71.30.+h

## I. INTRODUCTION

The discovery[1–3] of a coexistence of ferromagnetism and superconductivity in $RuSr_2Ln_{1.5}Ce_{0.5}Cu_2O_{10}$ and $RuSr_2LnCu_2O_8$ with $Ln$=Gd, Sm, or Eu has triggered a large amount of research activities in the field of such ruthenocuprates. These systems exhibit ferromagnetic order at a relatively high Curie temperature of about 100–140 K and become superconducting at a significantly lower critical temperature of about 15–40 K depending on the synthesis method. It is even more interesting to note that the ferromagnetic order coexists with superconductivity below the superconducting temperature. This suggests that pair breaking due to magnetic interactions is not significant in this system. These systems are characterized by the presence of both Ru-O and Cu-O planes in the unit cell; it has been speculated that the Ru-O plane is responsible for ferromagnetism, while superconductivity arises from the Cu-O planes as in the more conventional high-temperature superconductors, allowing the two phenomena to be decoupled. Mössbauer spectroscopy[3] and muon-spin-resonance[4] studies indeed support the idea concerning magnetism. In contrast, the origin of superconductivity in these as well as other cuprates has remained a controversial issue.

It is interesting to note here that the underlying electronic structure responsible for superconductivity is easily influenced by a small extent of substitutions. For example, while $RuSr_2Ln_{1.5}Ce_{0.5}Cu_2O_{10}$ is superconducting, a further substitution of $Ln$ by Ce, as in $RuSr_2LnCeCu_2O_{10}$, the system is not only nonsuperconducting, but also nonmetallic. This is most likely to be due to a change in the charge carrier concentration, since Ce can be in the tetravalent state, while lanthanide ion is generally found to be in the trivalent ($Ln^{3+}$) state. However, it becomes less obvious when we note that both Sm and Eu can exist also in the divalent state as well as in the trivalent state, just the way Ce can exist both as $Ce^{4+}$ and $Ce^{3+}$. Thus, the issue of doping of charge carriers into the system depends critically on the valency of these rare-earth ions. Additionally, it is *a priori* not obvious whether the doped charges, if any, would reside in the Cu-O planes or the Ru-O planes or even shared between the two, given the complexity of such a multicomponent system. It is therefore apparent that a careful study of the electronic structure of these compounds will be useful to address these important questions. Here we investigate the electronic structure of a series of related compounds along with a superconducting ruthenocuprate using x-ray photoelectron spectroscopy (XPS). XPS has already proven to be one of the most effective tools to study the electronic structure of such strongly correlated systems and to provide information concerning the site-specific valence states. Here we report the investigation of $RuSr_2EuCeCu_2O_{10}$ and $RuSr_2Eu_{1.5}Ce_{0.5}Cu_2O_{10}$. $RuSr_2EuCeCu_2O_{10}$ is a stoichiometric ruthenocuprate with a ferromagnetic transition at about 150 K, but is not superconducting. On the other hand, substitution of Ce ions by Eu ions forming $RuSr_2Eu_{1.5}Ce_{0.5}Cu_2O_{10}$, presumably doping charge carriers into the stoichiometric nonmetallic $RuSr_2EuCeCu_2O_{10}$ makes the system superconducting with a transition temperature of about 30 K. Most likely valence states of various elements in $RuSr_2EuCeCu_2O_{10}$ are $Ru^{5+}$, $Eu^{3+}$, $Ce^{4+}$, and $Cu^{2+}$, though other valence states, such as $Ru^{4+}$, $Ru^{6+}$, $Cu^{1+}$, $Cu^{3+}$, $Eu^{2+}$, and $Ce^{3+}$ are also known to exist. Assuming that valence states of the rare-earth ions continue to remain as before, namely $Eu^{3+}$ and $Ce^{4+}$, the substitution of Ce by Eu implies doping of 0.5 holes per formula unit; this may affect the valence state of either Ru or Cu or both. Therefore, we study two reference samples, namely $Sr_2RuO_4$ and $RuSr_2GdO_6$, where Ru is known to be in 4+ and 5+ states, respectively. Besides understanding the valence states, and consequently the nature of doping, in the superconducting ruthenocuprate, we analyze the Cu $2p$ spectra in terms of a configuration interaction approach within a $(CuO_4)^{6-}$ cluster model that takes into account the full multiplet interactions within Cu $2p$ and $3d$ levels,[5] providing us a quantitative description of the electronic structure.[6]

 

## II. EXPERIMENTAL AND CALCULATIONAL DETAILS

Polycrystalline samples of $RuSr_2Eu_{1.5}Ce_{0.5}Cu_2O_{10}$, $RuSr_2EuCeCu_2O_{10}$, and $RuSr_2GdO_6$ were synthesized by the solid state reaction method at ambient pressures. The details of the synthesis procedures are described elsewhere.[7,8] Polycrystalline samples of $Sr_2RuO_4$ were synthesized by the conventional ceramic route using stoichiometric quantities of high purity $SrCO_3$ and ruthenium oxide. They were thoroughly ground and the mixture was heated at 600 °C for 24 h to avoid Ru evaporation, then at 930 °C for 24 h, then at 1050 °C for 24 h, and finally at 1200 °C for 36 h with intermittent grindings. The product was then pressed into pellets and finally sintered at 1200 °C for 36 h and cooled to room temperature in air.[9] Magnetization measurements were performed on a SQUID magnetometer. Electron spectroscopic measurements were carried out in a custom-built multitechnique electron spectrometer manufactured by VSW, United Kingdom.[10] All the measurements were performed at about 150 K and at a base pressure of $7\times10^{-10}$ mbar. The sample surfaces were cleaned *in situ* by repeated scraping using a diamond file and carefully monitoring the C 1*s* and O 1*s* core level spectra as well as the reproducibility of all other spectra. All spectra were recorded with AlK$\alpha$ radiations with a total resolution of about 1.0 eV. Binding energy scale in each case was calibrated with the Fermi energy of silver sample in electrical contact with the sample. In each case, we looked for any evidence of charging by changing the x-ray power over a wide range. It was found that all spectra were free from charging effects.

Cluster calculations were carried out for the Cu 2*p* spectral features taking into account the full multiplet interactions within the $(CuO_4)^{6-}$ cluster. The O 2*p* to Cu 3*d* charge transfer energy is defined by $\Delta$ and the multiplet-averaged Cu 3*d*-3*d* interaction energy by $U_{dd}$. The multiplet-averaged Coulomb repulsion energy between the Cu 2*p* and Cu 3*d* holes is given by *Upd*. The hopping matrix elements between Cu 3*d* and O 2*p* orbitals are expressed in terms of Slater-Koster parameters $pd\sigma$ and $pd\pi$. The ratio $pd\sigma/pd\pi$ is fixed at 2. The ratio of $Upd/U_{dd}$ is fixed at 1.2. The multiplet coupling between the Cu 2*p* holes and Cu 3*d* holes is included using Slater integrals $F^2$, $G^1$, and $G^3$, whose values were set to 80% of the calculated atomic results.[11]

## III. RESULTS AND DISCUSSION

The quality of the sample in the case of ruthenocuprates is critical for a meaningful investigation, since impurity $SrRuO_3$ phase tends to form readily in the matrix. Observed (open circle) and fitted (line) x-ray patterns for both $RuSr_2Eu_{1.5}Ce_{0.5}Cu_2O_{10}$ and $RuSr_2EuCeCu_2O_{10}$ are shown in Fig. 1, suggesting well formed samples. Both the compounds form in $I4/mmm$ space group. The lattice parameters of $RuSr_2EuCeCu_2O_{10}$ are comparatively larger due to the higher content of larger-sized tetravalent Ce in comparison to trivalent Eu. The magnetization as a function of the temperature and the applied magnetic field is shown in Fig. 2 for both the samples. These compounds exhibit complex magnetic structures and we define $T_{mag}$ here as the temperature

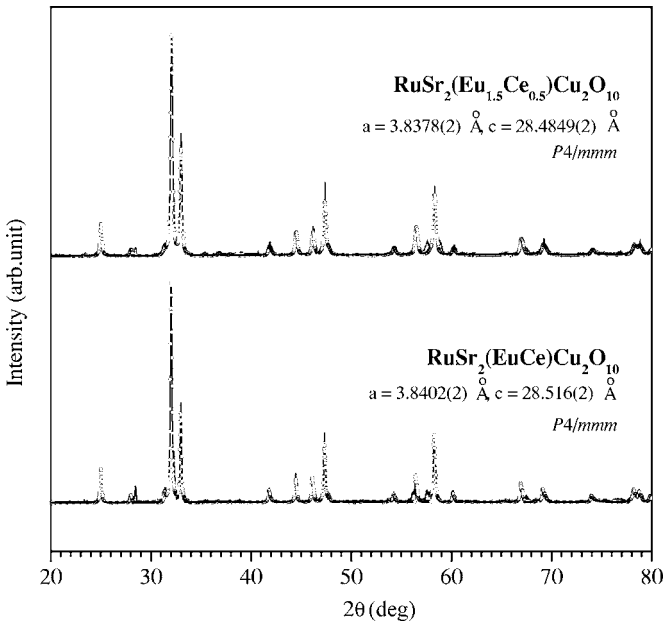


FIG. 1. Observed and fitted x-ray diffraction patterns for $RuSr_2Eu_{1.5}Ce_{0.5}Cu_2O_{10}$ and $RuSr_2EuCeCu_2O_{10}$.

corresponding to significant zero-field-cooled (ZFC) and field-cooled (FC) branching of the magnetization. $RuSr_2Eu_{1.5}Ce_{0.5}Cu_2O_{10}$ shows a $T_{mag}$ of about 100 K. The $RuSr_2EuCeCu_2O_{10}$ sample shows a higher magnetic transition temperature of about 150 K. Both the compounds exhibited clear ferromagnetic magnetization loops below magnetic transition temperatures with a reasonable coercive field ($H_c$) and a remnant magnetization ($M_r$). Representative magnetization loops for $RuSr_2Eu_{1.5}Ce_{0.5}Cu_2O_{10}$ at 5 K and 20 K are

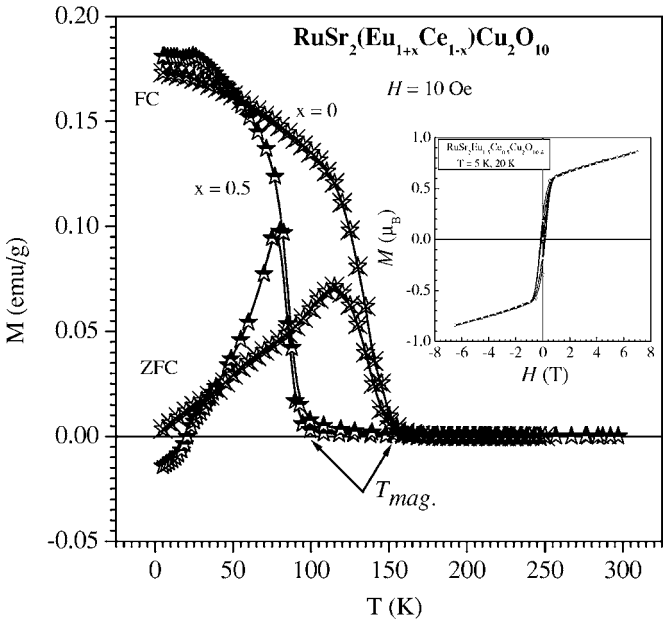


FIG. 2. Magnetization, $M$, as a function of temperature, $T$, for $RuSr_2Eu_{1.5}Ce_{0.5}Cu_2O_{10}$ (half solid stars) and $RuSr_2EuCeCu_2O_{10}$ (open crossed stars). Inset shows the $M$ vs $H$ plots at 5 and 20 K for the former.

shown for an applied field up to ±7 T in the inset of Fig. 2. $RuSr_2Eu_{1.5}Ce_{0.5}Cu_2O_{10}$ shows a superconducting transition at about 30 K, as also evidenced by the diamagnetism exhibited by the sample below this temparature in the ZFC plot. In contrast, $RuSr_2EuCeCu_2O_{10}$ is insulating through out the temperature region. Further physical characterizations including detailed magnetotransport, magnetization, thermoelectric power, and lattice expansion of both the samples are presented in Refs. 7 and 8.

While x-ray diffraction and magnetization measurements establish the bulk properties, x-ray photoelectron spectra have exponentially decaying information from the interior of the sample, therefore being essentially governed by the surface region with a few tens of Angstroms thickness. Thus, it becomes particularly important to ensure that impurities, often found on the surface, do not contribute significantly to the experimentally observed spectra. Surface cleanliness is normally achieved by scraping the sample *in situ*, exposing a clean surface. However, this requires a well-sintered, hard sample with strong intergrain bonding. In absence of this, scraping does not expose a clean surface by breaking open the individual grains; instead scraping such samples remove the grains as a whole, exposing new grain boundary regions which invariably contain substantial impurity phases. In this context, it is interesting to note that earlier reported[12,13] core level spectroscopic study of related compounds found presence of extensive carbon signal and intense multiple peaks associated with O 1*s* spectra spread over many electron volts; such features are often associated with the presence of impurities on the surfaces of the samples. In view of the obvious importance of surface cleanliness, we recorded O 1*s* spectra from the ruthenocuprates. These spectra shown in Fig. 3(a) are similar with one main peak at about 529 eV with a weak shoulder at 531.3 eV; specifically, the multiple intense peaks observed for O 1*s* in the earlier studies are totally absent in our results, suggesting a relatively clean sample surface. The cleanliness of the sample is further established by the absence of any C 1*s* signal, as will be shown later in Fig. 5. Another important check against impurity is the single species nature of Sr spectra, since Sr tends to appear as a carbonate in the grain boundary with a distinctly different binding energy. Figure 3(b) shows the Sr 3*d* region recorded for the superconducting as well as the nonsuperconducting compounds. Both the spectra have two distinct features separated by about 1.6 eV which corresponds to Sr $3d_{3/2}$ and Sr $3d_{5/2}$, even though the relative intensities of the two peaks are somewhat different. This is because Eu 4*d* feature overlaps with the Sr 3*d* features making it difficult to extract the exact Sr contributions. Hence we recorded the Sr $3p_{3/2}$ spectra as well for both the compounds and these are shown in the inset to Fig. 3(b). We clearly see in Sr $3p_{3/2}$ spectra that the spectral features and the peak positions are the same in both the superconducting and the nonsuperconducting compounds and is typical of Sr in the divalent state.

Figure 4 shows the core level photoemission spectra of Eu 3*d* and Ce 3*d* levels of $RuSr_2Eu_{1.5}Ce_{0.5}Cu_2O_{10}$ and $RuSr_2EuCeCu_2O_{10}$. Eu 3*d* spectra, shown in Fig. 4(a), exhibit two distinct features at 1163.1 eV and 1133.2 eV binding energies. These correspond to Eu $3d_{3/2}$ and Eu $3d_{5/2}$, respectively, with a spin-orbit splitting of 29.9 eV. These

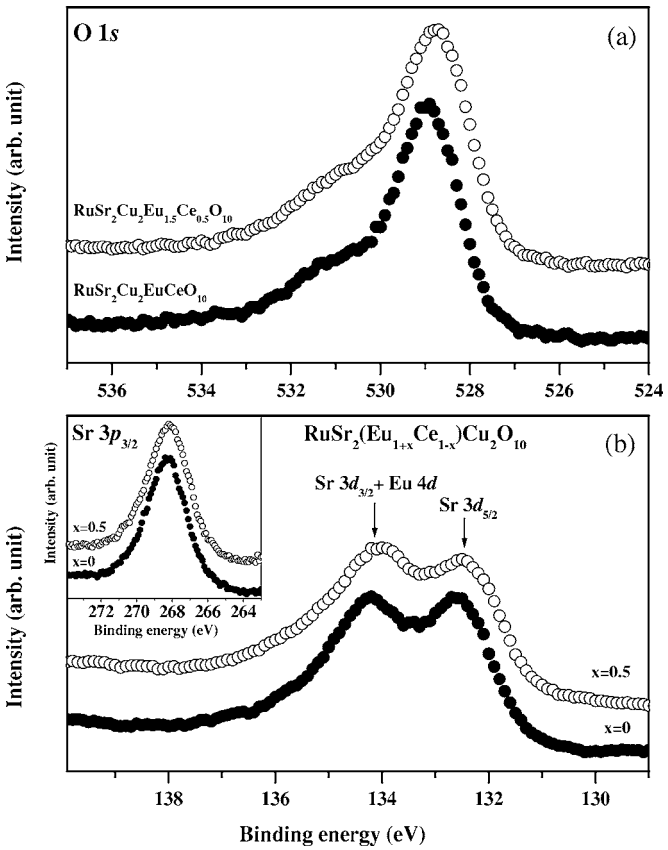


FIG. 3. Core level spectra of $RuSr_2Eu_{1.5}Ce_{0.5}Cu_2O_{10}$ (open circles) and $RuSr_2EuCeCu_2O_{10}$ (closed circles). O 1*s* and Sr 3*d* spectra are shown in panels (a) and (b), respectively. Sr $3p_{3/2}$ spectra for both the compounds are shown as an inset to panel (b).

values are in good agreement with the earlier reports[14] on $Eu^{3+}$ systems. It is well known that the 3*d* core level XPS of tetravalent ($4f^0$) Ce compounds exhibits a distinctive and complex spectrum, which is drastically different from the spectral features of trivalent ($4f^1$) compounds, thereby providing an easy identification of the valence state. The core level spectra of trivalent compounds exhibit a doublet feature arising from a main $4f^1$ and a weaker $4f^2$ shake-down peaks with an energy separation of 2–6 eV associated with each of the spin-orbit split core level features, $3d_{5/2}$ and $3d_{3/2}$. Specifically, in the case of the trivalent Ce oxide, it is reported[15–17] that the two peaks are of nearly the same intensity with a separation of 4.3 eV, while the spin-orbit split doublets are separated by 18 eV. In contrast, tetravalent Ce oxides exhibit for each of the Ce 3*d* spin-orbit peaks two sharp and intense peaks separated by about 16 eV together with a relatively broad feature in between. The Ce 3*d* spectra from both the compounds studied here are shown in Fig. 4(b). The features appearing between 900–916 eV belong to the $3d_{3/2}$ spin-orbit component and those between 881–897 eV to the $3d_{5/2}$ component. It is evident from the figure that the spectral features in Fig. 4(b) agree well with those of Ce 3*d* core level XPS spectra of tetravalent Ce compounds,[18] confirming the existence of $Ce^{4+}$ states in both the compounds.

Having established the valence states of the rare-earth ions, we now address the issue concerning the valence

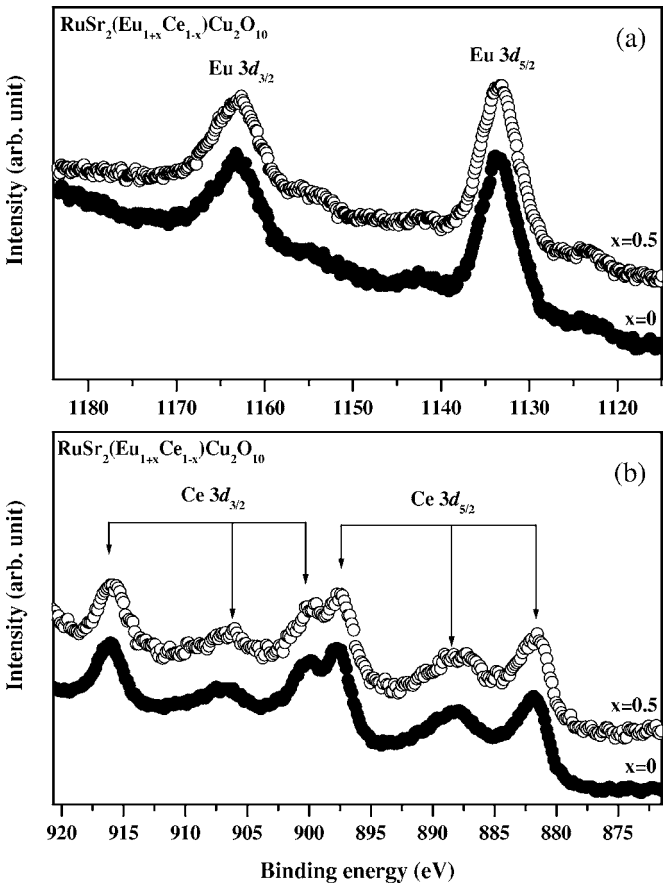


FIG. 4. Eu 3*d* and Ce 4*f* spectra of $RuSr_2Eu_{1.5}Ce_{0.5}Cu_2O_{10}$ (open circles) and $RuSr_2EuCeCu_2O_{10}$ (closed circles) are shown in panels (a) and (b), respectively.

state of the two transition metal ions, Ru and Cu, in the stoichiometric, $RuSr_2EuCeCu_2O_{10}$, and doped, $RuSr_2Eu_{1.5}Ce_{0.5}Cu_2O_{10}$. We have carefully analyzed the Ru 3*d* levels of the superconducting and nonsuperconducting samples, along with two reference samples, namely $RuSr_2GdO_6$ with $Ru^{5+}$ and $Sr_2RuO_4$ with $Ru^{4+}$ states, shown in Figs. 5(a)–5(d). Clearly, the spectra represent several overlapping features. One can easily identify the Sr $3p_{1/2}$ peak at about 278.5 eV and the main Ru related, spin-orbit split doublet $3d_{5/2}$ and $3d_{3/2}$ peaks in the energy window of 282–290 eV. Additionally, one can decipher weaker, higher binding energy components by the changing asymmetry of the higher binding energy sides of Ru 3*d* doublet features. Based on our quantitative analysis of the individual spectrum in terms of spectral decompositions into components, we believe that these low intensity spectral features are many-body satellite transitions associated with the main Ru 3*d* peaks, as has been reported earlier.[19,20] While in each case, satellite spectral features can be seen, spectral differences between $Sr_2RuO_4$ reported here and earlier is most probably due to the differences in the resolutions of the experimental setup. The spectral analysis was carried out within the following scheme. Each peak was represented by a symmetric function generated by a Lorentzian function convoluted with a Gaussian. The Lorentzian function represents the lifetime broadening effect, while the Gaussian function is supposed to account for all other broadenings including resolution broadenings. Besides one such function for the Sr $3p_{1/2}$, two more doublets were used, one doublet for the main Ru 3*d* spin-orbit split peaks and the other for the weak satellite features, with the intensity ratio between the spin-orbit split components being fixed at 1.5, determined by the degeneracy ratio. The energy separations between the peaks for both the doublets (spin-orbit splittings) were constrained to be the same. The lifetime effects for a specific core level for a given element is the same, so the full width at half maximum, $\gamma = 2\Gamma$, in the Lorentzian function is constrained to be same for the doublets. Also, $\sigma$ in the Gaussian function which represents the instrumental resolution is also constrained to be the same for all peaks. A background which is assumed to be proportional to the area under the photoemission signal prior to any inelastic scattering is also included in the fitting pro-

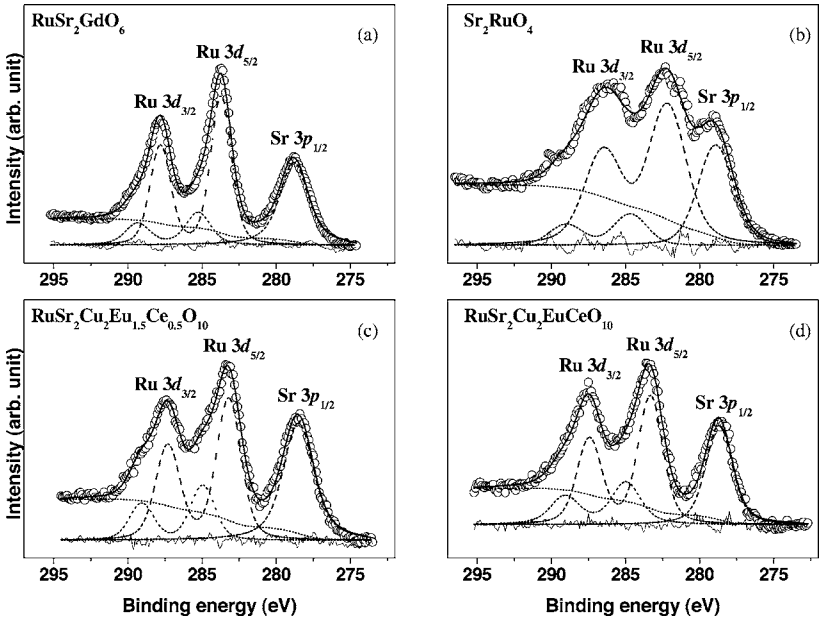


FIG. 5. Ru 3*d* spectra for $RuSr_2GdO_6$, $Sr_2RuO_4$, $RuSr_2Eu_{1.5}Ce_{0.5}Cu_2O_{10}$, and $RuSr_2EuCeCu_2O_{10}$ are shown in sections (a), (b), (c), and (d), respectively. Open circles show the experimental spectra, closed circles show the fitting, and thin solid line shows the difference between the two. Dashed line shows Ru 3*d* doublet with a spin orbit splitting of 4 eV and an intensity ratio of 1:1.5. Dashed-dotted lines show the Sr $3p_{1/2}$ component, short dotted line shows the background, and dotted lines, the satellite features of Ru 3*d*.

TABLE I. Parameters obtained from Ru 3*d* spectral analysis. $I_{Sr}/I_{Rutotal}$: ratio of the Sr 3*p* and Ru 3*d* total spectral intensities; $\Delta E_{spin\ orbit}$: spin orbit splitting of the Ru 3*d* levels; Ru $\Delta E_{satellite}$: separation between the Ru and the corresponding satellite peaks; $I_{satellite}/I_{main}$: ratio of the intensities between the Ru 3*d* satellite and the main peaks.

| Compound name | Sr 3*p* B.E. (eV) | Ru $3d_{5/2}$ B.E. (eV) | $\Delta E_{spin\ orbit}$ (eV) | Ru $\Delta E_{satellite}$ (eV) | $I_{satellite}/I_{main}$ |
|---|---|---|---|---|---|
| $RuSr_2GdO_6$ | 278.8 | 283.7 | 4.1 | 1.6 | 0.28 |
| $RuSr_2Cu_2Eu_{1.5}Ce_{0.5}O_{10}$ | 278.5 | 283.3 | 4.1 | 1.8 | 0.38 |
| $RuSr_2Cu_2EuCeO_{10}$ | 278.6 | 283.4 | 4.1 | 1.7 | 0.40 |
| $Sr_2RuO_4$ | 278.8 | 282.3 | 4.3 | 1.6 | 0.18 |

cedure. The results of these spectral decompositions are shown in Fig. 5, with the corresponding parameters summarized in Table I. The open circles show the experimental spectra, the solid line shows the fitted spectra, and the thin solid line shows the difference between the experimental spectra and the fitting. Dashed line shows Ru 3*d* doublet with a spin-orbit splitting of about 4 eV. Thin dashed lines show the Sr $3p_{1/2}$ component and the short dotted lines illustrate the doublet corresponding to the satellite feature of Ru 3*d* peaks. It is to be noted that none of these spectra shows any C 1*s* signal in contrast to earlier reports. Ru $3d_{3/2}$ and $3d_{5/2}$ main peaks in $RuSr_2GdO_6$ [Fig. 5(a)] appear at binding energies of 287.7 eV and 283.6 eV, respectively. The corresponding Ru 3*d* peaks for the $Sr_2RuO_4$ spectrum in Fig. 5(b) appear shifted by about 1.4 eV to the lower binding energy side, consistent with the lower valent $Ru^{4+}$ state in $Sr_2RuO_4$ compared to $Ru^{5+}$ state in $RuSr_2GdO_6$. Ru 3*d* spectra for the superconducting and the nonsuperconducting samples shown in Figs. 5(c) and 5(d), respectively, clearly exhibit peak positions at about the same binding energies as that for $RuSr_2GdO_6$, establishing conclusively that Ru exists in the pentavalent state in both these systems. The pentavalency of Ru in $RuSr_2Eu_{1.5}Ce_{0.5}Cu_2O_{10}$, $RuSr_2EuCeCu_2O_{10}$, and $RuSr_2GdO_6$ in contrast to tetravalent Ru in $Sr_2RuO_4$ is further indicated by the slight increase in the spin-orbit splitting, $\Delta E_{S-O}$, and somewhat lower satellite intensity for $Sr_2RuO_4$ compared to the other three compounds, as shown in Table I. In order to ensure that these conclusions are not vitiated by the complex, multiparameter spectral decomposition procedure, we have also recorded Ru 3*p* core level spectra from these compounds, which are shown in Fig. 6. Evidently the 3*p* peaks confirm the present interpretation with the Ru 3*p* peak from $Sr_2RuO_4$ appearing nearly an electron

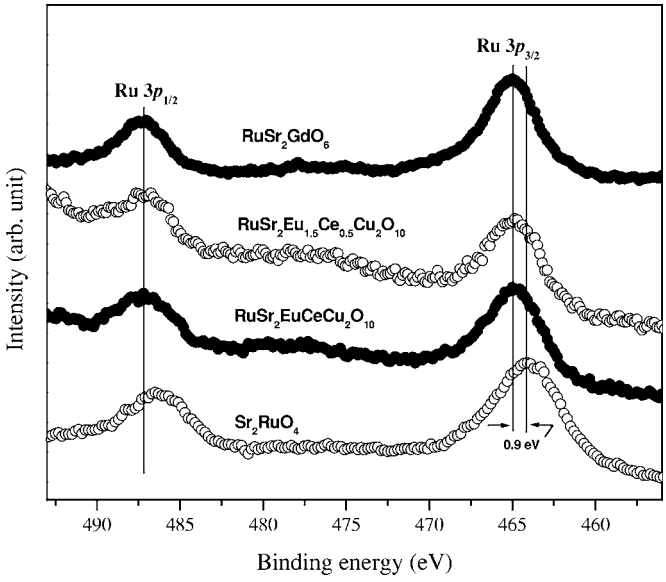


FIG. 6. Ru 3*p* spectra for $RuSr_2GdO_6$, $RuSr_2Eu_{1.5}Ce_{0.5}Cu_2O_{10}$, $RuSr_2EuCeCu_2O_{10}$, and $Sr_2RuO_4$.

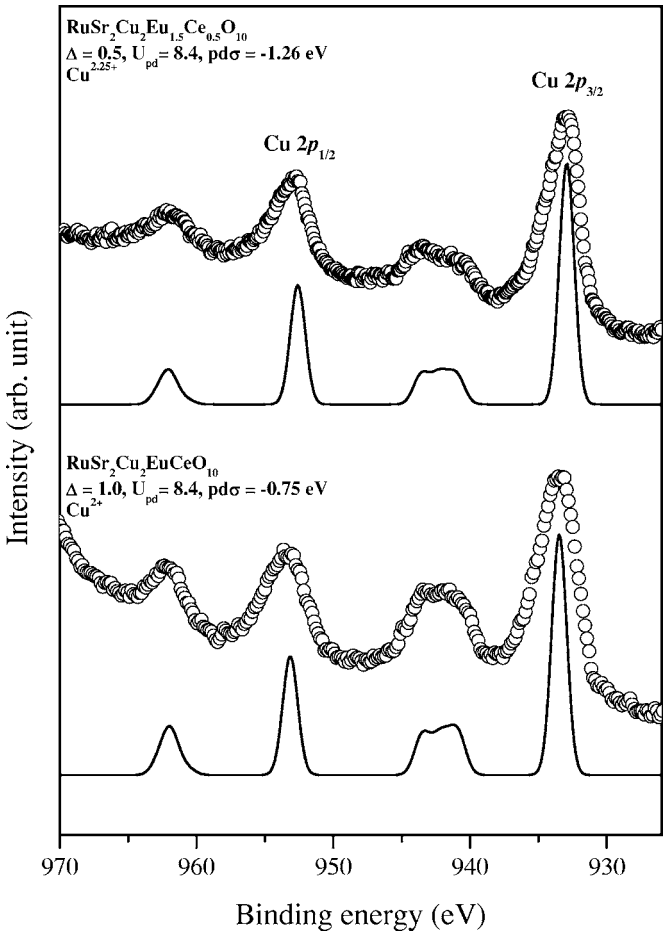


FIG. 7. Cu 2*p* spectra of $RuSr_2Eu_{1.5}Ce_{0.5}Cu_2O_{10}$ and $RuSr_2EuCeCu_2O_{10}$ are shown as open circles. The solid line shows the cluster calculations performed using a $(CuO_4)^{6-}$ cluster and including the full multiplet interactions.

volt below for the other three compounds consistent with the results in Fig. 5 and previous results[21] obtained from x-ray absorption measurements. The constancy of Ru valency with doping of charge carriers that brings about an insulator to metal transition and the superconducting state suggests that the electronic structure and transport properties in these compounds are not governed by the Ru-O plane, but by the Cu-O plane.

In order to understand the basic electronic structure of this family of compounds, we have recorded the Cu $2p$ spectra from these two compounds. Experimental Cu $2p$ spectra, shown in Fig. 7 with open circles, exhibit main $2p_{1/2}$ and $2p_{3/2}$ peaks along with two satellite features, characteristic of materials with a dominant $d^9$ configuration in the ground state.[6] The distinctive and different line shapes of the satellite features accompanying the $2p_{3/2}$ and $2p_{1/2}$ main signals are due to different multiplet structures associated with the $2p_{3/2}$ and $2p_{1/2}$ states arising from $2p^53d^9$ interactions. From the experimental spectra, we estimated the satellite-to-main peak intensity ratios to be 0.42 and 0.56 for $RuSr_2Eu_{1.5}Ce_{0.5}Cu_2O_{10}$ and $RuSr_2EuCeCu_2O_{10}$, respectively; the average satellite-to-main peak energy separations, defined by the centroids of these spectral features, are found to be 9.5 and 8.7 eV, respectively. The changes in these two quantities underline the difference in the basic electronic structure between the two compounds. In order to obtain a quantitative description and understanding of the electronic structure, we carried out cluster calculations to simulate Cu $2p$ for both the systems; the details of the calculation scheme can found in Ref. 5. The calculated spectra that simulate the experimental results best within realistic ranges of parameter values are shown by solid lines in Fig. 7. For the nonsuperconducting sample, O $2p$ to Cu $3d$ charge transfer energy, $\Delta$, is obtained as 1 eV, Cu $3d$ multiplet-averaged Coulomb repulsion energy, $U_{dd}$, as 7 eV, and the Slater-Koster parameters for hopping, $pd\sigma$, between Cu $3d$ and O $2p$ as 1.12 eV. The calculated intensity ratio and the average energy separation of the correlation satellite with respect to the main peak for this set of parameters are 0.51 and 8.8 eV, in good agreement with the experimental results. For the superconducting sample we obtained $\Delta=0.5$ eV, $U_{dd}=7$ eV, $pd\sigma=1.26$ eV. The intensity ratio and the energy separation of the correlation satellite with respect to the main peak are 0.40 and 9.5 eV in agreement with the experimental values. Here $\Delta \ll U_{dd}$, establishing the compounds to be deep in the charge transfer regime.[22] It is to be noted here that the specific calculation here does not involve any O $2p$ bandwidth; consequently, the charge-transfer energy, $\Delta$, is effectively measured from the middle of O $2p$ bandwidth. Noting that the O $2p$ bandwidth is expected to be larger than 2 eV, a $\Delta$ of 1 eV in the undoped compound places it in the effectively negative $\Delta$ or covalent insulator regime.[22] A hole doped into this system, as in the superconducting compound ensures that the doped hole would have a strongly hybridized O $2p$-Cu $3d$ character, residing to a large extent on the neighboring oxygen sites. This trend is further enhanced by a decrease of $\Delta$ to 0.5 eV in the doped system. This scenario is clearly suggested by the insensitivity of the Cu $2p$ binding energy and the spectral shapes to the doping, with the changes in the underlying electronic structure manifesting itself only in terms of subtle changes in the relative intensity and position of the satellite features compared to the main peaks.

## IV. CONCLUSION

Using photoelectron spectroscopy, we have investigated two ruthenocuprates, namely superconducting $RuSr_2Eu_{1.5}Ce_{0.5}Cu_2O_{10}$ and nonsuperconducting $RuSr_2EuCeCu_2O_{10}$ together with two reference compounds, namely $RuSr_2GdO_6$ and $Sr_2RuO_4$, to determine the valency of Ru in the ruthenocuprates. Our results show that Eu and Ce in both ruthenocuprates are in 3+ and 4+ states, respectively. Careful analysis of the Ru core level spectra from these ruthenocuprates suggest that the existence of a satellite feature of about $1.7\pm0.1$ eV higher binding energy from the main core level peak in all the oxides studied here. Ru in both ruthenocuprates is shown to be in the 5+ state, suggesting that the doped holes arising from the substitution of $Ce^{4+}$ by $Eu^{3+}$ in the superconducting sample resides in the Cu-O plane giving rise to its superconductivity, much as in the case of other high-$T_C$ cuprates. Analysis of Cu $2p$ core level spectra in terms of a cluster model, including configuration interaction and multiplet interactions between Cu $3d$ and $2p$ as well as that within the Cu $3d$ states, establish a close similarity of the basic electronic structure of these ruthenocuprates to those of other high-$T_C$ cuprates, establishing the nonsuperconducting $RuSr_2EuCeCu_2O_{10}$ as a small or even an effectively negative-$\Delta$ insulator, and suggesting that the doped hole in the superconducting sample would have a large weight on the neighboring oxygen sites.

## ACKNOWLEDGMENTS

This work was supported by Board of Research in Nuclear Sciences and the Department of Science and Technology, Government of India. U.M. thanks the Council of Scientific and Industrial Research, Government of India for financial support. Authors from NPL appreciate the interest and advice of Vikram Kumar in the present work.

*Also at Jawaharlal Nehru Centre for Advanced Scientific Research, Bangalore 560064, India. Electronic address: sarma@sscu.iisc.ernet.in

[1] L. Bauernfeind, W. Widder, and H. F. Braun, Physica C **254**, 151 (1995).

[2] L. Bauernfeind, W. Widder, and H. F. Braun, J. Low Temp. Phys. **105**, 1605 (1996).

[3] I. Felner, U. Asaf, Y. Levi, and O. Millo, Phys. Rev. B **55**, R3374 (1997).

[4] C. Bernhard, J. L. Tallon, Ch. Niedermayer, Th. Blasius, A.

Golnik, E. Brucher, R. K. Kremer, D. R. Noakes, C. E. Stronach, and E. J. Ansaldo, Phys. Rev. B **59**, 14099 (1999).
[5] K. Okada, A. Kotani, K. Maiti, and D. D. Sarma, J. Phys. Soc. Jpn. **65**, 1844 (1996).
[6] D. D. Sarma and A. Taraphder, Phys. Rev. B **39**, 11570 (1989).
[7] R. Lal, V. P. S. Awana, M. Peurla, Rajeev Rawat, V. Ganesan, H. Kishen, A. V. Narlikar, and R. Laiho, J. Phys.: Condens. Matter **18**, 2563 (2006).
[8] V. P. S. Awana, S. Balamurugan, L. S. Sharath Chandra, A. Deshpande, V. Ganesan, H. Kishen, E. Takayama-Muromachi, and A. V. Narlikar, Solid State Commun. **138**, 452 (2006).
[9] Sugata Ray, Ph.D. thesis, Indian Institute of Science, 2003.
[10] S. R. Barman and D. D. Sarma, Phys. Rev. B **49**, 13979 (1994).
[11] G. van der Laan and I. W. Kirkman, J. Phys.: Condens. Matter **4**, 4189 (1992).
[12] B. H. Frazer, Y. Hirai, M. L. Schneider, S. Rast, M. Onellion, U. Asaf, I. Felner, A. Reginelli, L. Perfetti, D. Ariosa, and G. Margaritondo, Phys. Rev. B **62**, 6716 (2000).
[13] B. H. Frazer, Y. Hirai, M. L. Schneider, S. Rast, M. Onellion, I. Nowik, I. Felner, S. Roy, N. Ali, A. Reginelli, L. Perfetti, D. Ariosa, and G. Margaritondo, Eur. Phys. J. B **19**, 177 (2001).
[14] L. C. Gupta, E. V. Sampathkumaran, R. Vijayaraghavan, Varsha Prabhawalkar, P. D. Prabhawalkar, and B. D. Padalia, Phys. Rev. B **23**, 4283 (1981).
[15] Manju U., S. R. Krishnakumar, S. Ray, S. Raj, M. Onoda, C. Carbone, and D. D. Sarma, Proc.-Indian Acad. Sci., Chem. Sci. **115**, 499 (2003).
[16] D. D. Sarma and C. N. R. Rao, J. Electron Spectrosc. Relat. Phenom. **20**, 25 (1980).
[17] D. D. Sarma, M. S. Hegde, and C. N. R. Rao, J. Chem. Soc., Faraday Trans. 2 **77**, 1509 (1981).
[18] D. D. Sarma, Ph.D. thesis, Indian Institute of Science, 1981.
[19] K. Okada, Surf. Rev. Lett. **9**, 1023 (2002).
[20] Hyeong-Do Kim, Han-Jin Noh, K. H. Kim, and S.-J. Oh, Phys. Rev. Lett. **93**, 126404 (2004).
[21] I. Felner, U. Asaf, C. Godart, and E. Alleno, Physica B **259–261**, 703 (1999).
[22] D. D. Sarma, J. Solid State Chem. **88**, 45 (1990); D. D. Sarma, H. R. Krishnamurthy, Seva Nimkar, P. P. Mitra, S. Ramasesha, and T. V. Ramakrishnan, Pramana, J. Phys. **38**, L531 (1992); Seva Nimkar, D. D. Sarma, H. R. Krishnamurthy, and S. Ramasesha, Phys. Rev. B **48**, 7355 (1993); Seva Nimkar, D. D. Sarma, and H. R. Krishnamurthy, *ibid.* **47**, 10927 (1993).